Research Square

Preprints are preliminary reports that have not undergone peer review.
They should not be considered conclusive, used to inform clinical practice,
or referenced by the media as validated information.

Flux-Activated Resonant Control of a Bosonic Quantum Memory

Yvonne Gao

yvonne.gao@nus.edu.sg

National University of Singapore https://orcid.org/0000-0002-6360-9679

Fernando Valadares

National University of Singapore

Aleksandr Dorogov

Centre for Quantum Technologies, National University of Singapore, Singapore https://orcid.org/0000-0003-2708-6409

Tanjung Krisnanda

National University of Singapore

May Chee Loke

National University of Singapore

Ni-Ni Huang

Centre for Quantum Technologies, National University of Singapore, Singapore https://orcid.org/0000-0002-7103-5935

Pengtao Song

Xi'an Jiaotong University https://orcid.org/0000-0001-7372-4331

Article

Keywords:

Posted Date: April 15th, 2026

DOI: https://doi.org/10.21203/rs.3.rs-9097048/v1

License: This work is licensed under a Creative Commons Attribution 4.0 International License.
Read Full License

Additional Declarations: There is **NO** Competing Interest.

Flux-Activated Resonant Control of a Bosonic Quantum Memory

Fernando Valadares,[1,*] Aleksandr Dorogov,[1,*] Tanjung Krisnanda,[1] May Chee Loke,[1] Ni-Ni Huang,[1] Pengtao Song,[1,†] and Yvonne Y. Gao[1,2,‡]

[1] *Centre for Quantum Technologies, National University of Singapore, Singapore*
[2] *Department of Physics, National University of Singapore, Singapore*

(Dated: March 11, 2026)

Universal control of bosonic degrees of freedom provides a hardware-efficient route for quantum information processing with high-dimensional systems. Bosonic circuit quantum electrodynamics (cQED), which leverages auxillary transmons to coherently control long-lived superconducting cavities, is well suited to this goal. However, such systems are traditionally operated in the dispersive regime, where the nearly degenerate cavity transitions prohibit the direct addressability of individual excitation levels of the bosonic mode and increase gate complexity. Here, we achieve direct oscillator control by dynamically accessing the resonant Jaynes–Cummings (JC) interactions, implemented with a hardware that integrates on-chip broadband magnetic flux delivery with a bosonic memory housed in a 3D superconducting cavity with lifetime exceeding 0.5 ms. We demonstrate deterministic preparation of Fock states and their superpositions within 100s of nanoseconds by directly climbing the JC ladder, and realise efficient arbitrary rotations between any pair of Fock states. Our resonant control scheme provides an analytical method for manipulating the entire Hilbert space of the bosonic mode at rates fundamentally more favourable than traditional dispersive strategies. This on-demand access to JC interactions opens a promising path toward realising robust Fock-basis qudits and harnessing the rich dynamics of high-dimensional bosonic systems for quantum information processing.

Effective control over a large Hilbert space is essential for both practical quantum information processing [1–3] and explorations of the rich underlying concepts of quantum physics [4–6]. A promising route towards this goal is to leverage the intrinsically large Hilbert space of quantum harmonic oscillators. Notably, bosonic circuit QED systems use 3D superconducting cavities coupled to auxillary transmons to realise highly controllable and coherent oscillators. Such devices have demonstrated Fock state preparation up to 100 photons [7] and cat states with an average photon population of 1024 [8]. Compared to parallel pursuits using discrete d-level systems (qudits) [9, 10], such as molecular spins [11, 12], optical photons [13, 14], trapped ions [15, 16], silicon nuclear spins [17] and superconducting artificial atoms [18–20], encoding information in higher levels of the oscillator does not introduce additional decoherence channels and is readily compatible with a broad range of existing bosonic quantum error correction schemes [21, 22].

In cQED systems, universal control of the bosonic mode is typically achieved via dispersive coupling to a nonlinear auxillary element, commonly in the form of a transmon qubit [23]. In this regime, oscillator transitions are close in frequency and not individually addressable, as illustrated (Fig. 1a). Therefore, arbitrary operations on the oscillator state often require driving the transmon and the cavity simultaneously with complex numerically optimised waveforms [24–26]. However, these numerical pulses are susceptible to parasitic dynamics, and their 'black-box' nature often complicates effective troubleshooting. Although operations can also be implemented using higher-order parametric processes without numerical optimization [27, 28], they are limited by the achievable coupling strength or drive-induced errors [29, 30]. Therefore, an analytical and versatile control method that directly addresses individual cavity transitions would fill an important gap for bosonic quantum information processing.

In this work, we use flux-activated resonant Jaynes-Cummings (JC) interactions to access number-selective cavity transitions and implement arbitrary yet analytically simple control of a bosonic memory mode. These dynamics are enabled by adjusting the transmon-cavity detuning on demand via a broadband on-chip flux line. This allows us to rapidly switch the coupled system between a highly nonlinear resonant dynamics with well-resolved JC transitions and the dispersive regime with suppressed cavity photon loss. We protect the coherence of the bosonic memory against flux line leakage by incorporating on-chip low-pass filtering over the frequency band occupied by the cavity and the transmon. As a result, the lifetime of the bosonic mode reaches $T_1 = 590 \pm 40\,\mu$s ($Q \sim 2.6 \times 10^7$) when the transmon is tuned to be dispersively coupled – more than a two-fold improvement over previous implementations using the magnetic hose [31, 32]. We leverage these hardware capabilities to demonstrate the direct creation of Fock states and their superpositions by sequentially climbing the JC ladder. Furthermore, we demonstrate state transfer between any two chosen energy levels of the cavity using multi-tone pulses and realise arbitrary rotations between them. This resonant control scheme can readily be

* Contributed equally to this work
† Current address: School of Automation Science and Engineering, Xi'an Jiaotong University, Xi'an 710049, China
‡ Corresponding author: yvonne.gao@nus.edu.sg

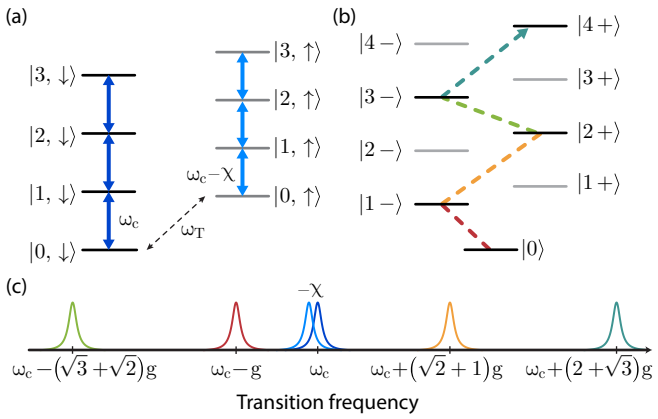

FIG. 1. **Comparison of the dispersive and resonant regimes**. **(a)** The bosonic transitions in the dispersive regime are degenerate within each qubit manifold and are separated by dispersive coupling strength, χ, between the $|\downarrow\rangle$ and $|\uparrow\rangle$ manifolds. **(b)** This degeneracy is lifted in the resonant JC regime, with level splittings $\propto g \gg \chi$, enabling fast selective excitation of individual bosonic levels. **(c)** The frequency spectra of both coupling regimes shown on the same axis.

applied to the general class of spin-boson systems, such as opto-acoustic modes coupled to artificial atoms [33] or motional degrees of freedom of ions controlled by a spin [34]. Thus, our results establish a valuable building block for efficient universal control and quantum information processing using bosonic modes in different physical platforms.

The resonant control technique explored in this work is based on the theoretical proposal by Strauch [35], which adiabatically connects the eigenstates of the resonant JC Hamiltonian to the product eigenbasis of the decoupled circuits. It improves upon earlier works [36, 37] that rely on sequentially turning on and off the spin-boson coupling.

The dynamics of a spin-boson system on resonance is well approximated within the rotating wave approximation by the JC Hamiltonian [38]

$$\hat{H}_{\mathrm{JC}} = g\left(\hat{a}^\dagger\hat{\sigma}^- + \hat{a}\hat{\sigma}^+\right), \tag{1}$$

where $\hat{a}$ ($\hat{a}^\dagger$) is the annihilation (creation) operator of the boson in the form of a superconducting cavity, $\hat{\sigma}^-$ ($\hat{\sigma}^+$) is the lowering (raising) Pauli operator of the spin, realised with a transmon qubit, and g is the coupling strength between them. The $\hat{H}_{\mathrm{JC}}$ eigenstates are the ground state $|0,\downarrow\rangle$ and the Nth-excited levels

$$|N\pm\rangle = \frac{1}{\sqrt{2}}\left(|N,\downarrow\rangle \pm |N{-}1,\uparrow\rangle\right), \tag{2}$$

where $|N,s\rangle$ is the product of the cavity Fock state $|N\rangle$ and the transmon state $|s=\downarrow,\uparrow\rangle$, with eigenfrequencies $\omega_{|N\pm\rangle} = \pm\sqrt{N}g$. This photon-number dependence of $\omega_{|N\pm\rangle}$ leads to the direct addressability of the transitions as illustrated in Fig. 1(b).

We are particularly interested in the red and blue JC sidebands

$$\begin{aligned} |N+\rangle &\overset{\omega_{N,r}}{\longleftrightarrow} |(N{+}1)-\rangle, \\ |N-\rangle &\overset{\omega_{N,b}}{\longleftrightarrow} |(N{+}1)+\rangle, \end{aligned} \tag{3}$$

with transition frequencies $\omega_{N,r} = -(\sqrt{N{+}1}{+}\sqrt{N})g$ and $\omega_{N,b} = (\sqrt{N{+}1}{+}\sqrt{N})g$ relative to the rotating frame, respectively. Transitions $\omega_{1,b}$, $\omega_{2,r}$, and $\omega_{3,b}$ are shown with orange, green, and teal, in Fig. 1. This set of transitions, together with ground state excitations $|0,\downarrow\rangle \leftrightarrow |1\pm\rangle$, can selectively connect any two eigenstates of the resonant JC Hamiltonian with a spectral resolution on the order of g (Fig. 1c). That makes the timescale of our protocol fundamentally more favourable compared to control schemes using the dispersive coupling, as discussed in [39].

To translate this fast control on the JC levels to effective operations on the bosonic mode alone, we simply need to adiabatically decrease the transmon frequency away from the cavity resonance. This transforms the coupled eigenstates in Eq. (2) into products of cavity and transmon eigenstates: $|N+\rangle \to |N,\downarrow\rangle$ and $|N-\rangle \to |N{-}1,\uparrow\rangle$. The red sidebands in Eq. (3) map to the transitions $|N,\downarrow\rangle \leftrightarrow |N,\uparrow\rangle$, similar to the standard transmon excitations in the dispersive regime [40]. In contrast, the blue sideband, $|N{-}1,\uparrow\rangle \leftrightarrow |N{+}1,\downarrow\rangle$, is only directly accessible in the resonant JC dynamics [35]. Therefore, the on-demand access to the resonant JC dynamics, together with the ability to adiabatically detune the transmon from the oscillator, allows us to orchestrate any desired operations on bosonic mode.

To leverage this resonant control scheme, we construct a new bosonic circuit QED hardware that can simultaneously provide strong and broadband flux control while protecting the cavity from decay (Fig. 2a). Our device features a superconducting stub cavity as the long-lived quantum memory coupled to a transmon qubit with a coupling strength $g/2\pi = 12.2 \pm 0.1\,\mathrm{MHz}$. It is combined with a lithographically defined on-chip flux line placed in close proximity to the SQUID loop with area $470\,\mu\mathrm{m}^2$. Flux delivery is highly efficient, featuring a mutual inductance of $0.387\,\Phi_0/\mathrm{mA}$. This allows us to minimise the loop area and hence reduce the impact of flux-noise on the transmon coherence times [39]. In this particular device, we measure transmon $T_1 \approx 23\,\mu\mathrm{s}$ and $T_2^{\mathrm{echo}} \approx 3.5\,\mu\mathrm{s}$ in the lower sweet spot. The flux line bandwidth reaches at least 1.3 GHz, allowing fast transmon frequency adjustment in the nanosecond timescale. Although we did not calibrate at higher frequencies due to the presence of a 2 GHz low-pass filter on the coaxial line, our finite-element simulations predict the bandwidth $\sim 4\,\mathrm{GHz}$, limited by the on-chip low-pass filter [39].

This CPW-based chip design is carefully optimised to reduce the energy loss of cavity and transmon through the flux line. In comparison to the microstrip flux line shown in a recent work [41], our strategy provides a more compact solution that allows convenient integration of additional circuits such as the readout resonator

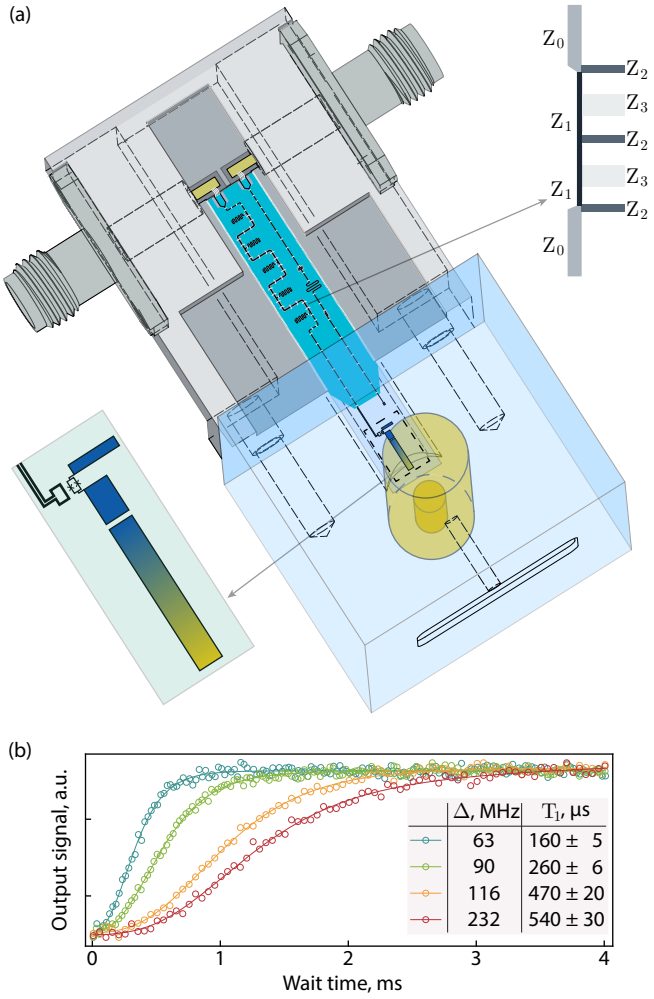

FIG. 2. **Architecture for robust flux-delivery in a high-Q bosonic circuit QED device**. **(a)** High-Q $\lambda/4$ coaxial cavity coupled to an asymmetric SQUID-transmon (shown in bottom-left inset). The flux bias is delivered by a transmission line wirebonded to an SMA port at the opposite end of the chip. The flux line and a readout resonator partially adopt a coplanar waveguide (CPW) architecture. They are equipped with two 3rd-order Chebyshev low-pass filters in series (schematics shown in top-right inset) and a Purcell filter, respectively, to protect the cavity and the transmon against decay. **(b)** The cavity T_1 is measured while the transmon is parked at a few selected flux points with different values of $\Delta = (\omega_{\rm cav} - \omega_{\rm T})/2\pi$, showing an increase in T_1 as the transmon-induced decay is suppressed at larger detunings.

and cascaded filtering on the same chip. We use two 3rd-order low-pass Chebyshev filters [42] with cutoff frequency of 4 GHz in series, schematically depicted in top-right inset of Fig. 1a. Based on finite element simulations, this structure achieves 98 dB attenuation at the cavity frequency of $\omega_{\rm cav}/2\pi = 6.868$ GHz and at least 50 dB attenuation in the transmon frequency range of $\omega_{\rm T}/2\pi = 5.894 - 7.634$ GHz. As a result, energy loss through the flux line is heavily suppressed for both quantum memory and transmon. We verify this by preparing the cavity in a coherent state and tracking the vacuum state $|0\rangle$ population over time at a few different cavity-transmon detunings as shown in Fig. 2b. The lifetime reaches a maximum of $T_1 = 590 \pm 40\,\mu$s at a detuning of $\Delta = (\omega_{\rm cav} - \omega_{\rm T})/2\pi = 260$ MHz, at which point the inverse-Purcell decay is suppressed. These photon loss values are comparable to those of typical 3D bosonic superconducting devices without flux integration.

Our device combines a highly coherent bosonic mode with fast tunability of a nonlinear auxiliary element, making it an ideal testbed for resonant control protocols. We first showcase the efficacy of this control framework by preparing arbitrary superpositions of Fock states with a set of analytical pulses. For example, we prepare $\frac{1}{\sqrt{2}}\left(|0\rangle| + |3\rangle\right)$ (Fig. 3a) using a pulse sequence consisting of a $\pi/2$-pulse from $|0\rangle$ to $|1+\rangle$ followed by two π-pulses to $|2-\rangle$ and $|3+\rangle$. The frequencies of each transition are determined using standard spectroscopy experiments, and the pulses durations are chosen to maximise the photon-number parity contrast after climbing each step of the JC ladder [39]. We calibrate the optimal speed of the adiabatic detuning by first preparing $|1+\rangle$ on resonance, followed by a flux pulse with a smooth, variable-duration ramp until the system is in a strong dispersive regime with $\Delta = 100$ MHz. We then directly measure the cavity $|1\rangle$ population using the photon-number-resolved spectroscopy and choose a minimal ramp duration of 200 ns that maximises the population of $|1\rangle$. We further showcase the ease of orchestrating arbitrary multi-component superpositions of Fock states by creating $\frac{1}{2}|0\rangle + \frac{\sqrt{3}}{\sqrt{8}}\left(i|2\rangle + |4\rangle\right)$ (Fig. 3b) using the same method. The phase of the superposition is implemented by simply changing the phase of the pulse addressing the corresponding transition. This technique can be directly used to create arbitrary logical states superpositions in the binomial encoding [43, 44]. The total pulse sequence to prepare the state in Fig. 3a (b) takes 640 ns (688 ns), and the corresponding fidelity of the final state is estimated as $93 \pm 3\%$ ($89 \pm 2\%$) from density matrix reconstruction [45, 46], limited by transmon decoherence [39].

As an alternative to sequentially climbing the JC ladder, several transitions can also be activated simultaneously to realise more complex dynamics. For instance, the analog of the spin angular momentum J_x over a subspace of dimension d of the JC Hamiltonian can be constructed by driving each transition with amplitude

$$A_n = 2\eta_n A\sqrt{n\,(d-n)}, \;\; 1 \le n < d, \tag{4}$$

where A is the overall pulse amplitude and η_n is an experimentally calibrated scaling factor of the drive strength associated to each transition [39]. Driving J_x for a total time of π/A enacts pairwise state transfers between target levels. Here we use this multi-tone drive to create Fock state $|5\rangle$ from the ground state. In principle, the optimal amplitudes of each spectral component can be analytically derived to implement a perfect state transfer [35]. In practice, to improve the fidelity beyond the

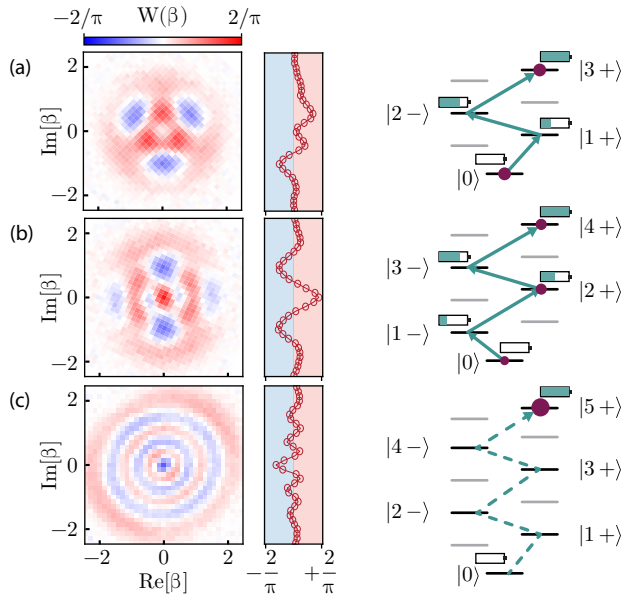

FIG. 3. **State preparation in the resonant regime.** Left panel: Normalised Wigner plots and 1D cuts along $\mathrm{Re}[\beta] = 0$ of states created using the flux-activated resonant interactions. Right panel: corresponding transitions activated to climb the JC ladder. **(a)** State $\frac{1}{\sqrt{2}}(|0\rangle + |3\rangle)$, and **(b)** state $\frac{1}{2}|0\rangle + \frac{\sqrt{3}}{\sqrt{8}}(i|2\rangle + |4\rangle)$ are created using sequential drives. **(c)** Fock state $|5\rangle$ created from vacuum by simultaneously driving multiple JC transitions. The progress bars illustrate the steps of state preparation, and the circles indicate the resulting Fock populations.

analytical solution, we allow A_n to assume complex values and obtain the amplitudes using a gradient descent algorithm which maximises the state preparation fidelity for a fixed time [35, 39]. We present, in Fig. 3c, the measured Wigner function of a Fock $|5\rangle$ prepared with this method using a 800 ns pulse. We obtain a state fidelity of $75 \pm 2\%$, limited by both the transmon decoherence and imperfect calibrations of η_n [39].

Furthermore, we use the multi-tone control to apply arbitrary rotations between two Fock states. This enacts Givens rotations on a qudit in Fock encoding: $\hat{\mathcal{R}}_{n_A,n_B}(\theta) = \exp[-i\theta/2(|n_A\rangle\langle n_B| + |n_B\rangle\langle n_A|)]$. Any arbitrary operation on a qudit can be constructed via a combination of $\hat{\mathcal{R}}_{n_A,n_B}(\theta)$ [35, 47], promising a simpler and faster control compared to the previous work [48]. Our implementation consists of resonantly transferring the population of a level $|n_A+\rangle$ to $|\,(n_B-1)\,-\rangle$, and then driving a transition from the latter state to $|n_B+\rangle$ with an effective rotation angle θ (Fig. 4a). The sequence is concluded with a second J_x applied in reverse, which swaps $|\,(n_B-1)\,-\rangle$ and $|n_A+\rangle$ populations while reverting spectator levels to their original configuration. After the transmon is adiabatically detuned, this operation is equivalent to a Givens rotation between the cavity levels $|n_A\rangle$ and $|n_B\rangle$ [47]. This operation can be naturally extended to perform gates in any chosen subspace, such as the logical states of the binomial encoding, as we demonstrate in [39]. As a concrete example, we apply Givens rotations $\hat{\mathcal{R}}_{1,4}(\theta)$ between Fock states $|1\rangle$ and $|4\rangle$. The parity of the final state is measured as a function of θ, showing a continuous evolution between a minimum value corresponding to $|1\rangle$ and a maximum corresponding to $|4\rangle$ (Fig. 4b). For $\theta = 0, \pi/4, \pi/2$ and π, we measure the full Wigner function of the cavity as shown in the plots in Fig. 4c. The density matrix reconstruction of the Wigner measurements indicates state fidelities of $80 \pm 2\%$, $76 \pm 2\%$, $71 \pm 2\%$, $68 \pm 2\%$, respectively. This is consistent with the numerical simulation with real experimental parameters [39].

The performance of the Givens rotation and state preparation are limited mainly by transmon dephasing, followed by coherent errors and transmon T_1 [39]. The effect of each decoherence channel can be understood in terms of the matrix element of JC levels with the corresponding jump operators. Interestingly, transmon pure dephasing does not lead to dephasing of the JC levels, as the corresponding jump operator $\hat{\sigma}_z$ has zero matrix element $\langle N \pm |\sigma_z| N\pm\rangle = 0$. Instead, it translates to depolarisation within each excitation manifold with corresponding matrix element $\langle N \pm |\sigma_z| N\mp\rangle = 1$.

In the limit of long coherence times of the memory mode, the energy decay of the resonant system is predominantly defined by the transmon relaxation rate corresponding to the jump operator $\hat{\sigma}^-$. The matrix elements defining the loss of energy are $\langle (N-1) \pm |\sigma^-| N\pm\rangle = \langle (N-1) \mp |\sigma^-| N\pm\rangle = 0.5$, indicating that the energy decay rate of the composite system is half that of the transmon regardless of N. In this implementation, the durations of the individual drives are limited by the effective lifetime of the system on resonance. This constraint results in coherent errors caused by leakages to spectator JC levels. A full master equation simulation with these error sources taken into account consistently reproduces experimental observations [39].

To enhance the overall fidelity of our resonant control scheme, we can readily adopt the known strategies to mitigate the decoherence of flux-tunable transmons, which is the dominant source of imperfection in this implemenation. For example, the transmon T_2 can be increased by reducing the flux sensitivity of the SQUID either by decreasing its area, increasing the asymmetry between the shunting Josephson junctions [39, 49], or using geometries that are inherently more noise-resilient [50]. At the same time, flux modulation can be used to engineer AC sweet spots at the cavity frequency to reduce the direct decoherence limit during the operations. Both strategies are supported by the large bandwidth and strong flux delivery of the on-chip line developed in this work. Besides greater T_2, increasing the transmon-cavity coupling strength g leads to more selective sideband transitions and faster adiabatic detuning, both of which can reduce the duration of the protocol and mitigate errors. Thus, the performance of the resonant operations shown in this work is not fundamentally limited by the control mech-

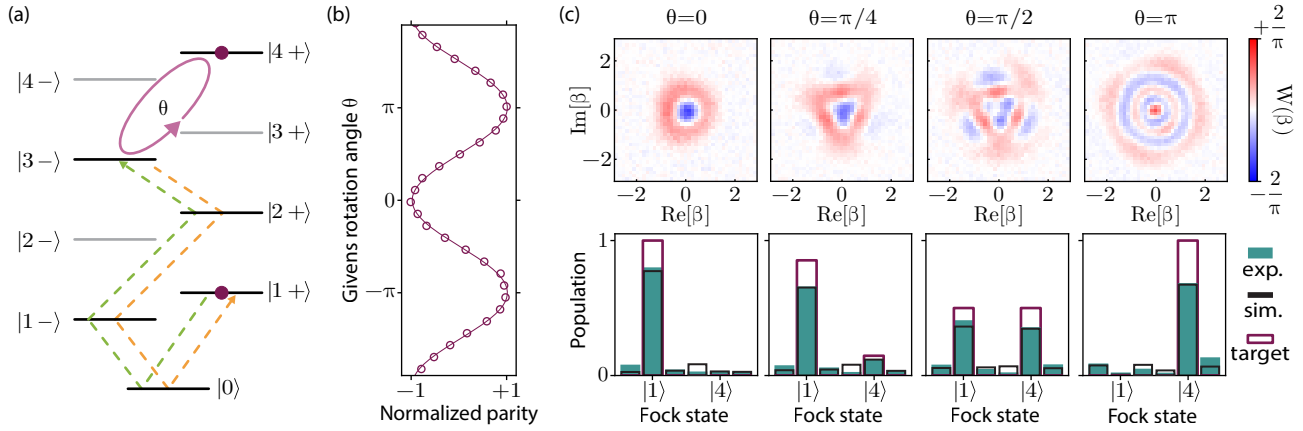

FIG. 4. **Givens rotation $\hat{\mathcal{R}}_{1,4}(\theta)$. (a)** The $|1+\rangle$ state population is swapped with $|3-\rangle$ state using a J_x pulse, which is then followed by a sideband pulse to $|4+\rangle$ with an effective rotation angle θ and a second J_x pulse that reverts the first swap. This sequence effectively implements a gate between states $|1+\rangle$ and $|4+\rangle$ that translates into a Givens rotation between Fock states $|1\rangle$ and $|4\rangle$ after adiabatic detuning. **(b)** Normalised final state parity measured for arbitrary rotation angle θ, showing that the protocol can create arbitrary superpositions of two Fock states. **(c)** Normalised Wigner function plots and Fock states populations of the cavity state for $\theta = 0, \pi/4, \pi/2$, and π. The population distributions are obtained from the reconstructed density matrices and consistent with both the ideal state (target) and the outcomes simulated with real experimental parameters (black).

anisms or our device architecture, and can be directly improved by further optimisation of device parameters.

In summary, our work demonstrates the control of a long-lived bosonic quantum memory through number-selective transitions in the JC Hamiltonian. This new capability is enabled by a robust flux-tunable architecture that can effectively switch the system between the dispersive and the resonant regimes. We prepare arbitrary superpositions of Fock states via either sequential or multi-tone sideband driving. Moreover, we use the JC transitions to efficiently implement arbitrary Givens rotations, providing a path for the universal control of qudits encoded in oscillators. Finally, thanks to the direct access to the JC levels, our protocol is intuitive and calibration-friendly. Moreover, it leverages a frequency selectivity that scales with the coupling factor g, allowing potentially faster control compared to typical dispersive operations and other parametrically activated techniques. Therefore, our work marks an important step towards more efficient control capabilities of long-lived microwave quantum memories in cQED and opens up new possibilities for quantum information processing with bosonic modes.

Acknowledgements We acknowledge the funding support from the Singapore Ministry of Education (T2EP50222-0017) and The University of Sydney - National University of Singapore 2026 Ignition Grants. F.V., A.D., N.H., acknowledge the support of the Singapore National Quantum Scholarship Scheme (NQSS). We thank Mr. Kyle Chu and Mr. Jean-Samuel Tettekpoe for their technical inputs during the project development. We thank Dr. Yao Lu and Dr. Mustafa Bakr for the valuable discussions during the writing of this manuscript.

[1] P. W. Shor, Scheme for reducing decoherence in quantum computer memory, Physical Review A **52**, R2493–R2496 (1995).
[2] S. Zhou, M. Zhang, J. Preskill, and L. Jiang, Achieving the heisenberg limit in quantum metrology using quantum error correction, Nature Communications **9**, 10.1038/s41467-017-02510-3 (2018).
[3] H.-Y. Huang, Y. Tong, D. Fang, and Y. Su, Learning Many-Body Hamiltonians with Heisenberg-Limited Scaling, Physical Review Letters **130**, 200403 (2023).
[4] E. Altman *et al.*, Quantum Simulators: Architectures and Opportunities, PRX Quantum **2**, 017003 (2021).
[5] W. Hofstetter and T. Qin, Quantum simulation of strongly correlated condensed matter systems, Journal of Physics B: Atomic, Molecular and Optical Physics **51**, 082001 (2018).
[6] D. A. Abanin *et al.*, Observation of constructive interference at the edge of quantum ergodicity, Nature **646**, 825–830 (2025).
[7] X. Deng, S. Li, Z.-J. Chen, Z. Ni, Y. Cai, J. Mai, L. Zhang, P. Zheng, H. Yu, C.-L. Zou, S. Liu, F. Yan, Y. Xu, and D. Yu, Quantum-enhanced metrology with large fock states, Nature Physics **20**, 1874–1880 (2024).
[8] O. Milul, B. Guttel, U. Goldblatt, S. Hazanov, L. M. Joshi, D. Chausovsky, N. Kahn, E. Çiftyürek, F. Lafont, and S. Rosenblum, Superconducting Cavity Qubit with Tens of Milliseconds Single-Photon Coherence Time, PRX Quantum **4**, 030336 (2023).

[9] B. P. Lanyon, M. Barbieri, M. P. Almeida, T. Jennewein, T. C. Ralph, K. J. Resch, G. J. Pryde, J. L. O'Brien, A. Gilchrist, and A. G. White, Simplifying quantum logic using higher-dimensional Hilbert spaces, Nature Physics **5**, 134–140 (2008).

[10] Y. Wang, Z. Hu, B. C. Sanders, and S. Kais, Qudits and High-Dimensional Quantum Computing, Frontiers in Physics **8:589504**, 10.3389/fphy.2020.589504 (2020).

[11] M. Rubín-Osanz, L. Bersani, S. Chicco, G. Allodi, R. De Renzi, A. Mavromagoulos, M. D. Roy, S. Piligkos, E. Garlatti, and S. Carretta, Implementation of the Quantum Fourier Transform on a molecular qudit with full refocusing and state tomography (2025), arXiv:2512.15611.

[12] E. Moreno-Pineda, C. Godfrin, F. Balestro, W. Wernsdorfer, and M. Ruben, Molecular spin qudits for quantum algorithms, Chemical Society Reviews **47**, 501–513 (2018).

[13] Y. Wang, S. Ru, F. Wang, P. Zhang, and F. Li, Experimental demonstration of efficient high-dimensional quantum gates with orbital angular momentum, Quantum Science and Technology **7**, 015016 (2021).

[14] B. Kim, K.-M. Hu, M.-H. Sohn, Y. Kim, Y.-S. Kim, S.-W. Lee, and H.-T. Lim, Qudit-based variational quantum eigensolver using photonic orbital angular momentum states, Science Advances **10**, 10.1126/sciadv.ado3472 (2024).

[15] P. J. Low, B. White, and C. Senko, Control and readout of a 13-level trapped ion qudit, npj Quantum Information **11**, 85 (2025).

[16] X. Shi, J. Sinanan-Singh, T. J. Burke, J. Chiaverini, and I. L. Chuang, Efficient Implementation of a Quantum Algorithm with a Trapped Ion Qudit (2025), arXiv:2506.09371.

[17] X. Yu, B. Wilhelm, D. Holmes, A. Vaartjes, D. Schwienbacher, M. Nurizzo, A. Kringhøj, M. R. v. Blankenstein, A. M. Jakob, P. Gupta, F. E. Hudson, K. M. Itoh, R. J. Murray, R. Blume-Kohout, T. D. Ladd, N. Anand, A. S. Dzurak, B. C. Sanders, D. N. Jamieson, and A. Morello, Schrödinger cat states of a nuclear spin qudit in silicon, Nature Physics **21**, 362–367 (2025).

[18] Z. Wang, R. W. Parker, E. Champion, and M. S. Blok, High-E_J/E_C transmon qudits with up to 12 levels, Physical Review Applied **23**, 034046 (2025).

[19] P. Liu, R. Wang, J.-N. Zhang, Y. Zhang, X. Cai, H. Xu, Z. Li, J. Han, X. Li, G. Xue, W. Liu, L. You, Y. Jin, and H. Yu, Performing SU(d) Operations and Rudimentary Algorithms in a Superconducting Transmon Qudit for $d = 3$ and $d = 4$, Physical Review X **13**, 021028 (2023).

[20] E. Champion, Z. Wang, R. W. Parker, and M. S. Blok, Efficient Control of a Transmon Qudit Using Effective Spin-7/2 Rotations, Physical Review X **15**, 021096 (2025).

[21] B. M. Terhal, J. Conrad, and C. Vuillot, Towards scalable bosonic quantum error correction, Quantum Science and Technology **5**, 043001 (2020).

[22] A. L. Grimsmo, J. Combes, and B. Q. Baragiola, Quantum computing with rotation-symmetric bosonic codes, Phys. Rev. X **10**, 011058 (2020).

[23] A. Blais, A. L. Grimsmo, S. M. Girvin, and A. Wallraff, Circuit quantum electrodynamics, Reviews of Modern Physics **93**, 025005 (2021).

[24] S. Krastanov, V. V. Albert, C. Shen, C.-L. Zou, R. W. Heeres, B. Vlastakis, R. J. Schoelkopf, and L. Jiang, Universal control of an oscillator with dispersive coupling to a qubit, Physical Review A **92**, 040303(R) (2015).

[25] R. W. Heeres, B. Vlastakis, E. Holland, S. Krastanov, V. V. Albert, L. Frunzio, L. Jiang, and R. J. Schoelkopf, Cavity State Manipulation Using Photon-Number Selective Phase Gates, Physical Review Letters **115**, 137002 (2015).

[26] R. W. Heeres, P. Reinhold, N. Ofek, L. Frunzio, L. Jiang, M. H. Devoret, and R. J. Schoelkopf, Implementing a universal gate set on a logical qubit encoded in an oscillator, Nature Communications **8**, 94 (2017).

[27] J. Huang, T. J. DiNapoli, G. Rockwood, M. Yuan, P. Narasimhan, E. Gupta, M. Bal, F. Crisa, S. Garattoni, Y. Lu, L. Jiang, and S. Chakram, Fast Sideband Control of a Weakly Coupled Multimode Bosonic Memory (2025), arXiv:2503.10623.

[28] T. Kim, T. Roy, X. You, A. C. Y. Li, H. Lamm, O. Pronitchev, M. Bal, S. Garattoni, F. Crisa, D. Bafia, D. Kurkcuoglu, R. Pilipenko, P. Heidler, N. Bornman, D. van Zanten, S. Zorzetti, R. Harnik, A. Murthy, A. Lunin, S. Belomestnykh, S. Zhu, C. Wang, A. Vallieres, Z. Huang, J. Koch, A. Grassellino, S. Chakram, A. Romanenko, and Y. Lu, Ultracoherent superconducting cavity-based multiqudit platform with error-resilient control (2025), arXiv:2506.03286.

[29] L. Verney, R. Lescanne, M. H. Devoret, Z. Leghtas, and M. Mirrahimi, Structural instability of driven josephson circuits prevented by an inductive shunt, Physical Review Applied **11**, 024003 (2019).

[30] Y. Lu, T. Zhao, A. Vallières, K. C. Smith, D. Weiss, X. You, Y. Zhang, S. Ganjam, A. Maiti, J. W. Garmon, *et al.*, Systematic construction of time-dependent hamiltonians for microwave-driven josephson circuits (2026), arXiv:2512.20743v3.

[31] F. Valadares, N.-N. Huang, K. T. N. Chu, A. Dorogov, W. Chua, L. Kong, P. Song, and Y. Y. Gao, On-demand transposition across light-matter interaction regimes in bosonic cQED, Nature Communications **15**, 5816 (2024).

[32] D. G. Atanasova, I. Yang, T. Hönigl-Decrinis, D. Gusenkova, I. Pop, and G. Kirchmair, In situ tunable interaction with an invertible sign between a fluxonium and a post cavity, PRX Quantum **6**, 020318 (2025).

[33] M. Bild, M. Fadel, Y. Yang, U. von Lupke, P. Martin, A. Bruno, and Y. Chu, Schrodinger cat states of a 16-microgram mechanical oscillator, Science **380**, 274–278 (2023), bild, Marius Fadel, Matteo Yang, Yu von Lupke, Uwe Martin, Phillip Bruno, Alessandro Chu, Yiwen eng 2023/04/20 Science. 2023 Apr 21;380(6642):274-278. doi: 10.1126/science.adf7553. Epub 2023 Apr 20.

[34] V. G. Matsos, C. H. Valahu, M. J. Millican, T. Navickas, X. C. Kolesnikow, M. J. Biercuk, and T. R. Tan, Universal quantum gate set for gottesman–kitaev–preskill logical qubits, Nature Physics **21**, 1664–1669 (2025).

[35] F. W. Strauch, All-Resonant Control of Superconducting Resonators, Physical Review Letters **109**, 210501 (2012).

[36] C. K. Law and J. H. Eberly, Arbitrary control of a quantum electromagnetic field, Physical review letters **76**, 1055 (1996).

[37] M. Hofheinz, H. Wang, M. Ansmann, R. C. Bialczak, E. Lucero, M. Neeley, A. O'connell, D. Sank, J. Wenner, J. M. Martinis, *et al.*, Synthesizing arbitrary quantum states in a superconducting resonator, Nature **459**, 546 (2009).

[38] E. T. Jaynes and F. W. Cummings, Comparison of quan-

tum and semiclassical radiation theories with application to the beam maser, Proceedings of the IEEE **51**, 89 (1963).
[39] Supplementary materials.
[40] D. I. Schuster, A. A. Houck, J. A. Schreier, A. Wallraff, J. M. Gambetta, A. Blais, L. Frunzio, J. Majer, B. Johnson, M. H. Devoret, S. M. Girvin, and R. J. Schoelkopf, Resolving photon number states in a superconducting circuit, Nature **445**, 515–518 (2007).
[41] Z. Li, E. Gupta, F. Zhao, R. Banerjee, Y. Lu, T. Roy, A. Oriani, A. Vrajitoarea, S. Chakram, and D. I. Schuster, A Cascaded Random Access Quantum Memory (2025), arXiv:2503.13953.
[42] D. M. Pozar, *Microwave engineering: theory and techniques* (John Wiley & Sons, 2021).
[43] M. H. Michael, M. Silveri, R. Brierley, V. V. Albert, J. Salmilehto, L. Jiang, and S. M. Girvin, New class of quantum error-correcting codes for a bosonic mode, Physical Review X **6**, 031006 (2016).
[44] P. Laha and P. van Loock, Arbitrary high-fidelity binomial codes from multiphoton spin-boson interactions, Physical Review Research **8**, 013237 (2026).
[45] T. Krisnanda, C. Y. Fontaine, A. Copetudo, P. Song, K. X. Lee, N.-N. Huang, F. Valadares, T. C. Liew, and Y. Y. Gao, Demonstrating efficient and robust bosonic state reconstruction via optimized excitation counting, PRX Quantum **6**, 010303 (2025).
[46] T. Krisnanda, P. Song, A. Copetudo, C. Y. Fontaine, T. Paterek, T. C. Liew, and Y. Y. Gao, Experimental demonstration of enhanced quantum tomography via quantum reservoir processing, Quantum Science and Technology **10**, 035041 (2025).
[47] G. K. Brennen, D. P. O'Leary, and S. S. Bullock, Criteria for exact qudit universality, Physical Review A **71**, 052318 (2005).
[48] B. Mischuck and K. Mølmer, Qudit quantum computation in the jaynes-cummings model, Physical Review A—Atomic, Molecular, and Optical Physics **87**, 022341 (2013).
[49] M. Hutchings, J. B. Hertzberg, Y. Liu, N. T. Bronn, G. A. Keefe, M. Brink, J. M. Chow, and B. Plourde, Tunable superconducting qubits with flux-independent coherence, Physical Review Applied **8**, 044003 (2017).
[50] J. Braumüller, M. Sandberg, M. R. Vissers, A. Schneider, S. Schlör, L. Grünhaupt, H. Rotzinger, M. Marthaler, A. Lukashenko, A. Dieter, *et al.*, Concentric transmon qubit featuring fast tunability and an anisotropic magnetic dipole moment, Applied Physics Letters **108** (2016).

Supplementary Files

This is a list of supplementary files associated with this preprint. Click to download.

- FARSupplementary.pdf